Published in final edited form as:
Angew Chem Int Ed Engl. 2010 May 17; 49(22): 3777–3781. doi:10.1002/anie.201000062.

Photothermal Effects of Supramolecularly Assembled Gold Nanoparticles for the Targeted Treatment of Cancer Cells**

Shutao Wang,
Department of Molecular and Medical Pharmacology, Crump Institute for Molecular Imaging (CIMI), California NanoSystems Institute (CNSI), Institute for Molecular Medicine (IMED), University of California, Los Angeles, 570 Westwood Plaza, Building 114, Los Angeles, CA 90095-1770, (USA), Fax: (+1)310-206-8975

Kuan-Ju Chen,
Department of Molecular and Medical Pharmacology, Crump Institute for Molecular Imaging (CIMI), California NanoSystems Institute (CNSI), Institute for Molecular Medicine (IMED), University of California, Los Angeles, 570 Westwood Plaza, Building 114, Los Angeles, CA 90095-1770 (USA), Fax: (+1)310-206-8975

Ting-Hsiang Wu,
Department of Electrical Engineering, University of California, Los Angeles, 420 Westwood Plaza, EIV 37-138, Los Angeles, CA 90095 (USA)

Hao Wang,
Department of Molecular and Medical Pharmacology, Crump Institute for Molecular Imaging (CIMI), California NanoSystems Institute (CNSI), Institute for Molecular Medicine (IMED), University of California, Los Angeles, 570 Westwood Plaza, Building 114, Los Angeles, CA 90095-1770 (USA), Fax: (+1)310-206-8975

Wei-Yu Lin,
Department of Molecular and Medical Pharmacology, Crump Institute for Molecular Imaging (CIMI), California NanoSystems Institute (CNSI), Institute for Molecular Medicine (IMED), University of California, Los Angeles, 570 Westwood Plaza, Building 114, Los Angeles, CA 90095-1770 (USA), Fax: (+1)310-206-8975

Minori Ohash,
Department of Molecular and Medical Pharmacology, Crump Institute for Molecular Imaging (CIMI), California NanoSystems Institute (CNSI), Institute for Molecular Medicine (IMED), University of California, Los Angeles, 570 Westwood Plaza, Building 114, Los Angeles, CA 90095-1770 (USA), Fax: (+1)310-206-8975

Pei-Yu Chiou [Prof.], and
Department of Mechanical and Aerospace Engineering, University of California, Los Angeles, 420 Westwood Plaza, EIV 37-138, Los Angeles, CA 90095 (USA)

Hsian-Rong Tseng [Prof.]
Department of Molecular and Medical Pharmacology, Crump Institute for Molecular Imaging (CIMI), California NanoSystems Institute (CNSI), Institute for Molecular Medicine (IMED), University of California, Los Angeles, 570 Westwood Plaza, Building 114, Los Angeles, CA 90095-1770 (USA), Fax: (+1)310-206-8975, Homepage: http://labs.pharmacology.ucla.edu/tsenglab/

**This research was supported by NIH-NCI NanoSystems Biology Cancer Center (U54CA119347).

Supporting information for this article is available on the WWW under http://dx.doi.org/10.1002/anie.201000062.

Shutao Wang: shutaowang@mednet.ucla.edu; Pei-Yu Chiou: pychiou@seas.ucla.edu; Hsian-Rong Tseng: hrtseng@mednet.ucla.edu

Keywords

gold; nanoparticles; photothermal effects; self-assembly; tumor therapy

Noble-metal nanostructures with unique photophysical properties have been considered as prime candidate agents for the photothermal treatment of cancer.[1–4] Typically, the photothermal properties of these nanostructures can be controlled by manipulating their sizes and shapes.[4,5] Over the past decade, significant endeavors have been devoted to the production of a variety of gold nanostructures, such as nanoparticles,[6,7] nanoshells,[8–10] nanorods,[11,12] and nanocages,[5,13,14] which are able to overcome limitations of organic-dye-based photothermal agents,[7] such as low light absorption and undesired photobleaching. For sufficient energy to be harvested/generated to damage tumor cells, the size of these nanostructure-based agents are required in the range of tens to hundreds nm.[15] However, the relatively "large" size of the agents often leads to poor bioclearance (i.e., accumulation in the liver, spleen, and kidneys), which is a major obstacle to their in vivo application.[16–18] Alternatively, the photophysical properties of noble-metal nanostructures can be altered systematically by the formation of aggregates through self-assembly.[19–30] The antibody-assisted aggregation of Au nanoparticles on cell membranes or in intracellular environments led to the enhancement of photothermal performance[31] as a result of the collective effects [32,33] associated with the assembled structures. Therefore, the self-assembly of small noble-metal building blocks, that is, noble-metal colloids with diameters of less than 8 nm[16–18] (compatible with renal clearance) would be a promising approach toward a new class of noble-metal photothermal agents.

Recently, we demonstrated a convenient, flexible, and modular self-assembly approach for the preparation of supramolecular nanoparticles (SNPs) of controlled size through multivalent molecular recognition based on β-cyclodextrin (CD) and adamantane (Ad) motifs.[34] Size-controlled SNPs were prepared by mixing three molecular building blocks: 1) an Ad-grafted polyamidoamine dendrimer with a diameter of approximately 1.9 nm, 2) CD-grafted branched polyethylenimine (CD-PEI), and 3) Ad-grafted polyethylene glycol (Ad-PEG). We hypothesized that such a supramolecular synthetic approach could be further explored to assemble inorganic building blocks (i.e., 2 nm Au colloids) into a collection of Au supramolecular nanoparticles (Au-SNPs) with defined sizes. We anticipated that the resulting Au-SNPs might exhibit enhanced photothermal effects[19] and could thus be promising candidate agents for photothermal cancer treatment. The use of a supramolecular approach enables[34,35] the convenient incorporation of targeting ligands to provide target-specific Au-SNPs.

In this study, we adopted a supramolecular approach to prepare size-controlled Au-SNPs for use as a new type of photothermal agent from three building blocks: Ad-grafted 2 nm Au colloids, CD-PEI, and Ad-PEG (Figure 1). We used transmission electron microscopy (TEM) and zeta-potential measurements to characterize the size/morphology and surface charge densities, respectively, of the resulting Au-SNPs. We carried out further studies to unveil the unique physical properties of the Au-SNPs, including 1) their stability at different temperatures and pH values, 2) their size-dependent photophysical properties, and 3) their thermally induced disassembly. Moreover, laser-induced microbubble-generation experiments were performed with the 118 nm Au-SNPs to demonstrate their significantly enhanced photothermal effects relative to those of the 2 nm Au colloids. We used arginine–glycine–aspartic acid (RGD) peptide as a targeting ligand and $\alpha_v\beta_3$-positive/negative cells as the corresponding biological system to test the specificity and selectivity of RGD-Au-SNPs, which were generated from

Au-SNPs by dynamic in situ ligand exchange,[35] and observed selective damage of the $\alpha_v\beta_3$-positive cells (no damage of neighboring $\alpha_v\beta_3$-negative cells).

The three molecular building blocks, Ad-grafted 2 nm Au colloids (Figure 2a), CD-PEI, and Ad-PEG, were prepared and characterized as shown in the Supporting Information. We then prepared size-controlled Au-SNPs (Figure 2b) by slowly adding phosphate-buffered saline (PBS, pH 7.2) with Ad-grafted 2 nm Au colloids (0.0213 $mgmL^{-1}$) to PBS solutions with variable amounts of CD-PEI (0.0725–5.73 $mgmL^{-1}$) and Ad-PEG (4.2 $mgmL^{-1}$), followed by incubation at room temperature overnight. By simply tuning the ratio between the Ad-grafted 2 nm Au colloids and CD-PEI, we were able to obtain a collection of Au-SNPs with variable sizes ranging between 40 and 118 nm (Figure 2c). The formation mechanism originally proposed for SNPs[34] can be used to explain the size controllability observed for Au-SNPs. In short, the mixing ratios of the three building blocks altered the equilibrium between the propagation/aggregation of the Au colloid/CD-PEI hydrogel network and the Ad-PEG-induced capping/solvation of the hydrogel network, and changes in this equilibrium led to changes in the size of the Au-SNPs.

TEM images indicated that the Au-SNPs had spherical shapes with a narrow size distribution (Figure 2b; see also the Supporting Information). Figure 2b shows a highly magnified typical TEM image of a single Au-SNP; individual 2 nm Au colloids are clearly visible. Zeta-potential measurements (Zetasizer Nano, Malvern Instruments) revealed that the Au-SNPs carried surface charge densities covering the range of 11–20 mV (see Figure S1 in the Supporting Information) as a result of the incorporation of positively charged CD-PEI. Since the Au-SNPs were prepared by supramolecular assembly, we characterized their dynamic stability under different environmental conditions. We monitored the size variation of 118 nm Au-SNPs in PBS by TEM[36] at temperatures ranging from 7 to 100°C (Figure 2d) and at pH values from 3 to 10 (Figure 2e). The results indicated that 118 nm Au-SNPs are stable in PBS at 7–40°C and pH 5–10. Also, Au-SNPs can maintain their size and morphology in PBS either with or without 10% serum, most likely because the “stealth” effect imparted by PEG grafted on the outside of the Au-SNPs could lower the further agglomeration of particles.[37] These results suggest that Au-SNPs can be used under physiological conditions. At higher temperatures (> 50°C, Figure 2d), they dissociated into small fragments, and a broader size distribution of the Au-SNPs was observed by TEM. Complete disassembly of the 118 nm Au-SNPs into 2 nm Au colloids was observed when the temperature was increased to 100°C. The thermal disassembly of 118 nm Au-SNPs can be attributed to the weakened Ad/CD supramolecular interactions at elevated temperatures.[38]

To test the feasibility of the application of Au-SNPs as photothermal agents, we chose 118 nm Au-SNPs as the model system.[39] For comparison, 2 nm Au colloids were employed as a control. First, we investigated the photophysical properties of 118 nm Au-SNPs and 2 nm Au colloids by UV/Vis spectroscopy (Figure 3a). Given the characteristic surface-plasmon-resonance absorption of Au-SNPs and Au colloids (between 500 and 530 nm),[19] we chose a 532 nm green pulsed laser to test their photothermal effects and performed laser-induced microbubble-generation studies to monitor the locally accumulated heat of individual Au-SNPs. We tested a broad range of energy densities (3–265 $mJcm^{-2}$) of a 532 nm pulsed laser with a 6 ns pulse duration. Au-SNPs and Au-colloid suspensions in PBS (with a normalized Au concentration of 4.67 $mgmL^{-1}$) were irradiated with the laser at different energies. For the 118 nm Au-SNPs, a laser threshold of 32 $mJcm^{-2}$ was sufficient for the generation of microbubbles upon laser irradiation (Figure 3b). In contrast, no microbubbles were observed for 2 nm Au colloids even at the maximum laser energy tested (265 $mJcm^{-2}$;Figure 3c). The significant enhancement of the photothermal effects in 118 nm Au-SNPs can be attributed to the collective heating effect[33] in Au-SNPs. Interestingly, we also found that the efficiency

of the collective heating effect was size-dependent: 40 nm Au-SNPs exhibited a threshold of 61 $mJcm^{-2}$.

The formation of explosive vapor bubbles on individual Au-SNPs requires an elevated local temperature higher than the critical temperature of the liquid medium (374°C for water).[40] We hypothesize that upon the formation of microbubbles, the localized accumulated heat could facilitate the thermal disassembly of Au-SNPs into smaller fragments, in a process similar to that observed for 118 nm Au-SNPs when the temperature was above 100°C (Figure 2d). To monitor laser-induced Au-SNP disassembly, we used a pulsed laser (with a 6 ns pulse duration) to irradiate Au-SNPs at a repetition rate of 1 Hz. Microbubble formation was captured by the time-resolved imaging setup 70 ns after the arrival of the laser pulse. We observed a dramatic decrease in the number of laser-induced microbubbles after irradiation with several laser pulses. Thus, most of the Au-SNPs in the solution appeared to have thermally disassembled into smaller fragments, which attenuates their photothermal characteristics.[7,19] In the following studies on photothermal treatment, a fixed laser power of 120 $mJcm^{-2}$ was used to ensure microbubble formation on the 118 nm Au-SNPs.

Through the incorporation of targeting ligands, photothermal agents based on Au nanostructures can be utilized for the targeted photothermal treatment of certain types of cancer cells.[6,12,41,42] In our study, RGD-Au-SNPs that could recognize tumor cells with membrane $\alpha_v\beta_3$ integrin receptors were produced by dynamic ligand exchange (Ad-PEG-RGD (0.21 mg) was added to a solution (1.0 mL) of 118 nm Au-SNPs (4.67 $mgmL^{-1}$); see the Supporting Information).[43] The 118 nm RGD-Au-SNPs were used along with the controls (RGD-grafted 2 nm Au colloids and nontargeting 118 nm Au-SNPs) for targeted photothermal treatment in four-well chamber slides containing both $\alpha_v\beta_3$-positive U87 glioblastoma cells and $\alpha_v\beta_3$-negative MCF7 breast cancer cells. To make it easier to visually distinguish the two different types of cells, we labeled the U87 and MCF7 cells with green and red fluorescent dyes (DiO and DiD cell-labeling solution, Invitrogen), respectively. After incubation for 20 min with the three agents and subsequent replacement of the culture media (to remove the free agents), the cells in the culture chambers were exposed to pulsed laser irradiation (6 ns, 120 $mJcm^{-2}$) with a beam diameter of 1 mm (a photomask was used; see the Supporting Information). The irradiated cells were kept in an incubator (5% CO_2, 37°C) for 2 h, during which time the cells damaged by microbubble formation could detach from the substrates. An inverted fluorescence microscope (Nikon TE2000) was employed to examine the cells within the irradiated regions. Cell detachment was observed for the U87 cells treated with RGD-Au-SNPs (Figure 4a). In contrast, negligible cell detachment was observed for MCF7 cells treated with RGD-Au-SNPs (Figure 4b) as well as for both types of cells treated with non-targeted Au-SNPs. These results suggest that 1) RGD peptide confers target specificity to the Au-SNPs to enable the photothermal treatment of $\alpha_v\beta_3$-positive U87 cells, and 2) nontargeting Au-SNPs have no significant effect on cancer cells, as their surface-grafted PEG chains[44] are capable of reducing nonspecific binding to cells. Furthermore, no cell detachment was detected for the U87 cells treated with Au colloids (Figure 4c); this result validated our previous observation that 2 nm Au colloids exhibit minute photothermal effects at the given pulsed laser irradiation.

To demonstrate the selectivity of RGD-Au-SNPs for target-specific photothermal treatment, we investigated the targeted depletion of $\alpha_v\beta_3$-positive cells in a cell mixture containing both $\alpha_v\beta_3$-positive U87 and $\alpha_v\beta_3$-negative MCF7 cells. We treated a 1:1 cell mixture (Figure 4d, middle) containing U87 cells (green) and MCF7 cells (red) with RGD-Au-SNPs (4.67 $mgmL^{-1}$). After the removal of free RGD-Au-SNPs, the cell mixture was irradiated with a pulsed laser. In the irradiated region, U87 cells (green) were depleted, and the remaining MCF7 cells (red) were able to be continuously cultured on the substrates (Figure 4d, right). In the region outside the laser footprint, both the positive and the negative cells remained. These results suggest that the photothermal treatment of RGD-Au-SNPs is highly selective for

targeted cells. Besides the specific targeting effects of RGD-Au-SNPs, the use of a pulsed laser led to effective photothermal effects in a defined location within a nanosecond time frame and thus enabled localized cell damage in a spatially confined fashion. In contrast, the previous use of continuous-wave radiation often led to a large area of cell damage as a result of heat diffusion from the targeted cells to the surrounding medium over the relatively long period of light irradiation.[45]

The cell-damage mechanism is based on the mechanical destruction associated with the formation of explosive microbubbles. It is similar to those proposed for photothermal agents based on Au nanoparticles[6,46,47] or carbon nanotubes,[48] but is dramatically different from the heating-damage mechanism observed for other photothermal agents.[7,8,41,49] To visualize the microbubble-induced mechanical destruction[46] of the targeted cell, we used time-resolved imaging to monitor how an RGD-Au-SNP-grafted cell responded to microbubble formation right after laser irradiation. To ensure that a small number of RGD-Au-SNPs were grafted on the cells, we treated the $\alpha_v\beta_3$-positive U87 cells with 118 nm RGD-Au-SNPs at low concentration (0.93 $mgmL^{-1}$). Figure 4e shows the time-dependant response of a U87 cell treated with RGD-Au-SNPs to irradiation with the 6 ns pulsed laser (120 $mJcm^{-2}$). After irradiation, a fast contraction of the cellular protrusion was observed as a result of the localized mechanical destruction caused by a microbubble.

In conclusion, we have successfully demonstrated the synthesis of size-controlled Au-SNPs from 2 nm Au colloids by a supramolecular self-assembly approach. The resulting Au-SNPs exhibited significantly enhanced photothermal effects and were used to demonstrate the targeted photothermal treatment of a subpopulation of cancer cells after the incorporation of target-specific ligands. We envision that 1) such a supramolecular assembly approach could be used to assemble other “small” inorganic nanoparticles (e.g., superparamagnetic oxide nanoparticles[50]) for broader application in materials science and biomedicine; 2) diverse functional building blocks and therapeutic loads (e.g., DNA, proteins, drugs) could be packaged into Au-SNPs, the laser-induced disassembly of which could be used as a controlled release mechanism; and 3) a two-photon laser[51] could be employed to overcome the tissue-penetration limitation.

Supplementary Material

Refer to Web version on PubMed Central for supplementary material.

References

1. Anderson RR, Parrish JA. Science 1983;220:524. [PubMed: 6836297]
2. Jain PK, Huang XH, El-Sayed IH, El-Sayed MA. Acc Chem Res 2008;41:1578. [PubMed: 18447366]
3. An K, Hyeon T. Nano Today 2009;4:359.
4. Lal S, Clare SE, Halas NJ. Acc Chem Res 2008;41:1842. [PubMed: 19053240]
5. Skrabalak SE, Chen J, Sun Y, Lu X, Au L, Cobley CM, Xia Y. Acc Chem Res 2008;41:1587. [PubMed: 18570442]
6. Lapotko DO, Lukianova E, Oraevsky AA. Laser Surg Med 2006;38:631.
7. Huang XH, Jain PK, El-Sayed IH, El-Sayed MA. Lasers Med Sci 2008;23:217. [PubMed: 17674122]
8. Gobin AM, Lee MH, Halas NJ, James WD, Drezek RA, West JL. Nano Lett 2007;7:1929. [PubMed: 17550297]
9. Hu KW, Liu TM, Chung KY, Huang KS, Hsieh CT, Sun CK, Yeh CS. J Am Chem Soc 2009;131:14186. [PubMed: 19772320]
10. Kim J, Park S, Lee JE, Jin SM, Lee JH, Lee IS, Yang I, Kim JS, Kim SK, Cho MH, Hyeon T. Angew Chem 2006;118:7918.Angew Chem Int Ed 2006;45:7754.

11. Dickerson EB, Dreaden EC, Huang XH, El-Sayed IH, Chu HH, Pushpanketh S, McDonald JF, El-Sayed MA. Cancer Lett 2008;269:57. [PubMed: 18541363]
12. Huang YF, Sefah K, Bamrungsap S, Chang HT, Tan W. Langmuir 2008;24:11860. [PubMed: 18817428]
13. Chen J, Wang D, Xi J, Au L, Siekkinen A, Warsen A, Li ZY, Zhang H, Xia Y, Li X. Nano Lett 2007;7:1318. [PubMed: 17430005]
14. Au L, Zheng D, Zhou F, Li ZY, Li X, Xia Y. ACS Nano 2008;2:1645. [PubMed: 19206368]
15. Lowery AR, Gobin AM, Day ES, Shah KY, Halas NJ, West JL. Clin Cancer Res 2005;11:9097s.
16. Mitragotri S, Lahann J. Nat Mater 2009;8:15. [PubMed: 19096389]
17. Choi HS, Liu W, Misra P, Tanaka E, Zimmer JP, Itty Ipe B, Bawendi MG, Frangioni JV. Nat Biotechnol 2007;25:1165. [PubMed: 17891134]
18. Nel AE, Madler L, Velegol D, Xia T, Hoek EMV, Somasundaran P, Klaessig F, Castranova V, Thompson M. Nat Mater 2009;8:543. [PubMed: 19525947]
19. Khlebtsov B, Zharov V, Melnikov A, Tuchin V, Khlebtsov N. Nanotechnology 2006;17:5167.
20. Lu ZD, Goebl J, Ge JP, Yin YD. J Mater Chem 2009;19:4597.
21. Zhuang J, Wu H, Yang Y, Cao YC. Angew Chem 2008;120:2240.Angew Chem Int Ed 2008;47:2208.
22. Troutman TS, Barton JK, Romanowski M. Adv Mater 2008;20:2604.
23. Ofir Y, Samanta B, Rotello VM. Chem Soc Rev 2008;37:1814. [PubMed: 18762831]
24. Elghanian R, Storhoff JJ, Mucic RC, Letsinger RL, Mirkin CA. Science 1997;277:1078. [PubMed: 9262471]
25. Lin S, Li M, Dujardin E, Girard C, Mann S. Adv Mater 2005;17:2553.
26. Katz E, Willner I. Angew Chem 2004;116:6166.Angew Chem Int Ed 2004;43:6042.
27. Cheng WL, Park NY, Walter MT, Hartman MR, Luo D. Nat Nanotechnol 2008;3:682. [PubMed: 18989335]
28. Maye MM, Lim IIS, Luo J, Rab Z, Rabinovich D, Liu TB, Zhong CJ. J Am Chem Soc 2005;127:1519. [PubMed: 15686385]
29. Niemeyer CM. Angew Chem 2001;113:4254.Angew Chem Int Ed 2001;40:4128.
30. Klajn R, Olson MA, Wesson PJ, Fang L, Coskun A, Trabolsi A, Soh S, Stoddart JF, Grzybowski BA. Nat Chem 2009;1:733.
31. Lapotko D, Lukianova E, Potapnev M, Aleinikova O, Oraevsky A. Cancer Lett 2006;239:36. [PubMed: 16202512]
32. Govorov AO, Richardson HH. Nano Today 2007;2:30.
33. Richardson HH, Carlson MT, Tandler PJ, Hernandez P, Govorov AO. Nano Lett 2009;9:1139. [PubMed: 19193041]
34. Wang H, Wang S, Su H, Chen KJ, Armijo AL, Lin WY, Wang Y, Sun J, Kamei K, Czernin J, Radu CG, Tseng HR. Angew Chem 2009;121:4408.Angew Chem Int Ed 2009;48:4344.
35. Wang H, Chen KJ, Wang ST, Ohashi M, Kamei KI, Sun J, Ha JH, Liu K, Tseng HR. Chem Commun 2010;46:1851.
36. It is well-known that the overall aggregate size as measured by dynamic light scattering (DLS) is much larger than the average size determined by TEM, especially for inorganic nanoparticlesShenhar R, Norsten TB, Rotello VM. Adv Mater 2005;17:657.We obtained the size distribution of Au-SNPs from TEM measurements.
37. Harris JM, Chess RB. Nat Rev Drug Discovery 2003;2:214.
38. Rekharsky MV, Inoue Y. Chem Rev 1998;98:1875. [PubMed: 11848952]
39. It is widely recognized that the diameter of nanoparticle therapeutics for cancer should be roughly in the range of 10–120 nmDavis ME, Chen Z, Shin DM. Nat Rev Drug Discovery 2008;7:771–782.
40. Kotaidis V, Plech A. Appl Phys Lett 2005;87
41. Pitsillides CM, Joe EK, Wei X, Anderson RR, Lin CP. Biophys J 2003;84:4023. [PubMed: 12770906]
42. Wang CG, Chen J, Talavage T, Irudayaraj J. Angew Chem 2009;121:2797.Angew Chem Int Ed 2009;48:2759.
43. Liu Z, Cai WB, He LN, Nakayama N, Chen K, Sun XM, Chen XY, Dai HJ. Nat Nanotechnol 2007;2:47. [PubMed: 18654207]

44. Harris, JM., editor. Poly(ethylene glycol) Chemistry: Biotechnical and Biomedical Applications. Plenum; New York: 1992.
45. O'Neal DP, Hirsch LR, Halas NJ, Payne JD, West JL. Cancer Lett 2004;209:171. [PubMed: 15159019]
46. Hleb EY, Hafner JH, Myers JN, Hanna EY, Rostro BC, Zhdanok SA, Lapotko DO. Nanomedicine 2008;3:647. [PubMed: 18817468]
47. Wu TH, Kalim S, Callahan C, Teitell MA, Chiou PY. Opt Express 2010;18:938. [PubMed: 20173916]
48. Kang B, Yu D, Dai Y, Chang S, Chen D, Ding Y. Small 2009;5:1292. [PubMed: 19274646]
49. Huang X, El-Sayed IH, Qian W, El-Sayed MA. J Am Chem Soc 2006;128:2115. [PubMed: 16464114]
50. Lee JH, Jun YW, Yeon SI, Shin JS, Cheon J. Angew Chem 2006;118:8340.Angew Chem Int Ed 2006;45:8160.
51. Starkey JR, Rebane AK, Drobizhev MA, Meng FQ, Gong AJ, Elliott A, McInnerney K, Spangler CW. Clin Cancer Res 2008;14:6564. [PubMed: 18927297]

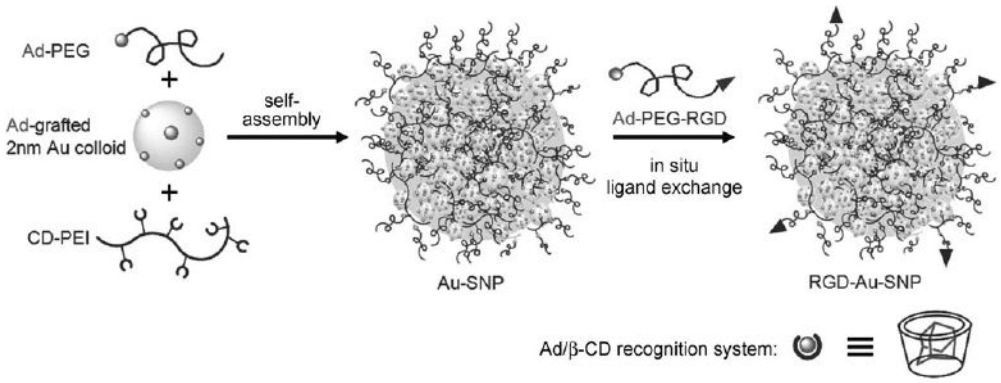

Figure 1.

Supramolecular synthetic approach for the preparation of size-controlled gold supramolecular nanoparticles (Au-SNPs). A molecular-recognition system based on adamantane (Ad) and β-cyclodextrin (CD) was employed to assemble three building blocks: Ad-grafted 2 nm Au colloids, CD-PEI, and Ad-PEG. Ad-PEG-RGD was introduced onto Au-SNPs by in situ ligand exchange to give RGD-Au-SNPs that could recognize a certain type of tumor cell with membrane $\alpha_v\beta_3$ integrin receptors.

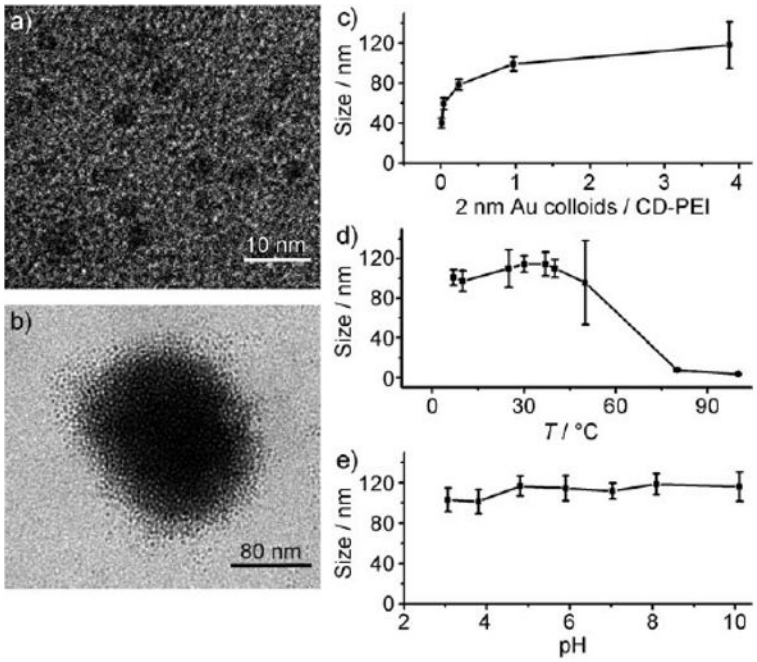

Figure 2.

Analysis by transmission electron microscopy (TEM). a) Ad-grafted 2 nm Au colloids: the inorganic building blocks of Au-SNPs. b) A single 118 nm Au-SNP obtained by the supramolecular synthetic approach. c) Titration plot showing the relationship between the size of Au-SNPs and the mixing ratio of the Au colloids and CD-PEI. d,e) Effect of temperature (d) and the pH value (e) on the stability of 118 nm Au-SNPs.

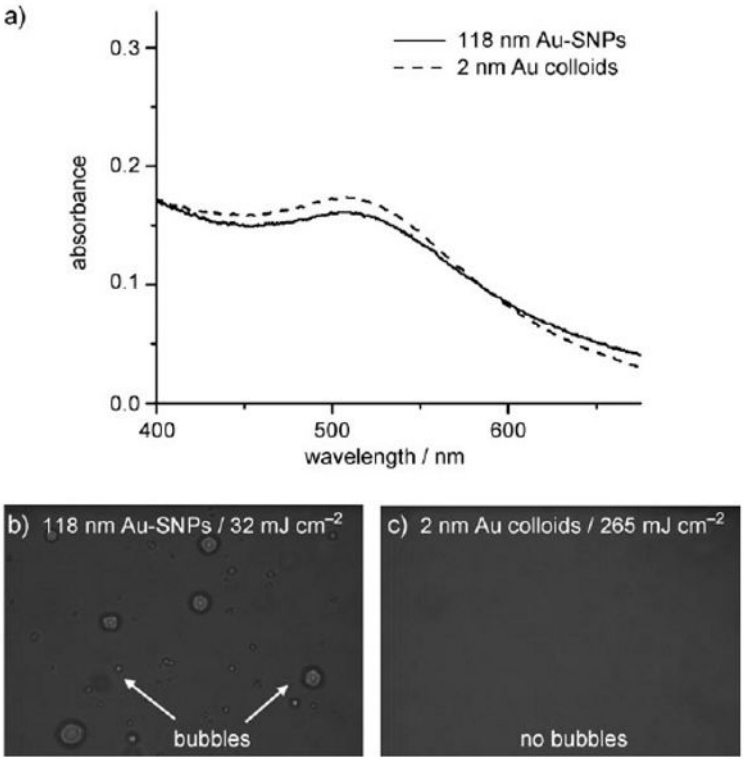

Figure 3.

a) UV/Vis absorption spectra of 2 nm Au colloids and 118 nm Au-SNPs. b,c) Time-resolved bright-field micrographs of suspensions of 118 nm Au-SNPs (b) and Ad-grafted 2 nm Au colloids (c) during the scanning of a pulsed laser (6 ns, 532 nm; 32 $mJcm^{-2}$ for 118 nm Au-SNPs and 265 $mJcm^{-2}$ for Ad-grafted 2 nm Au colloids).

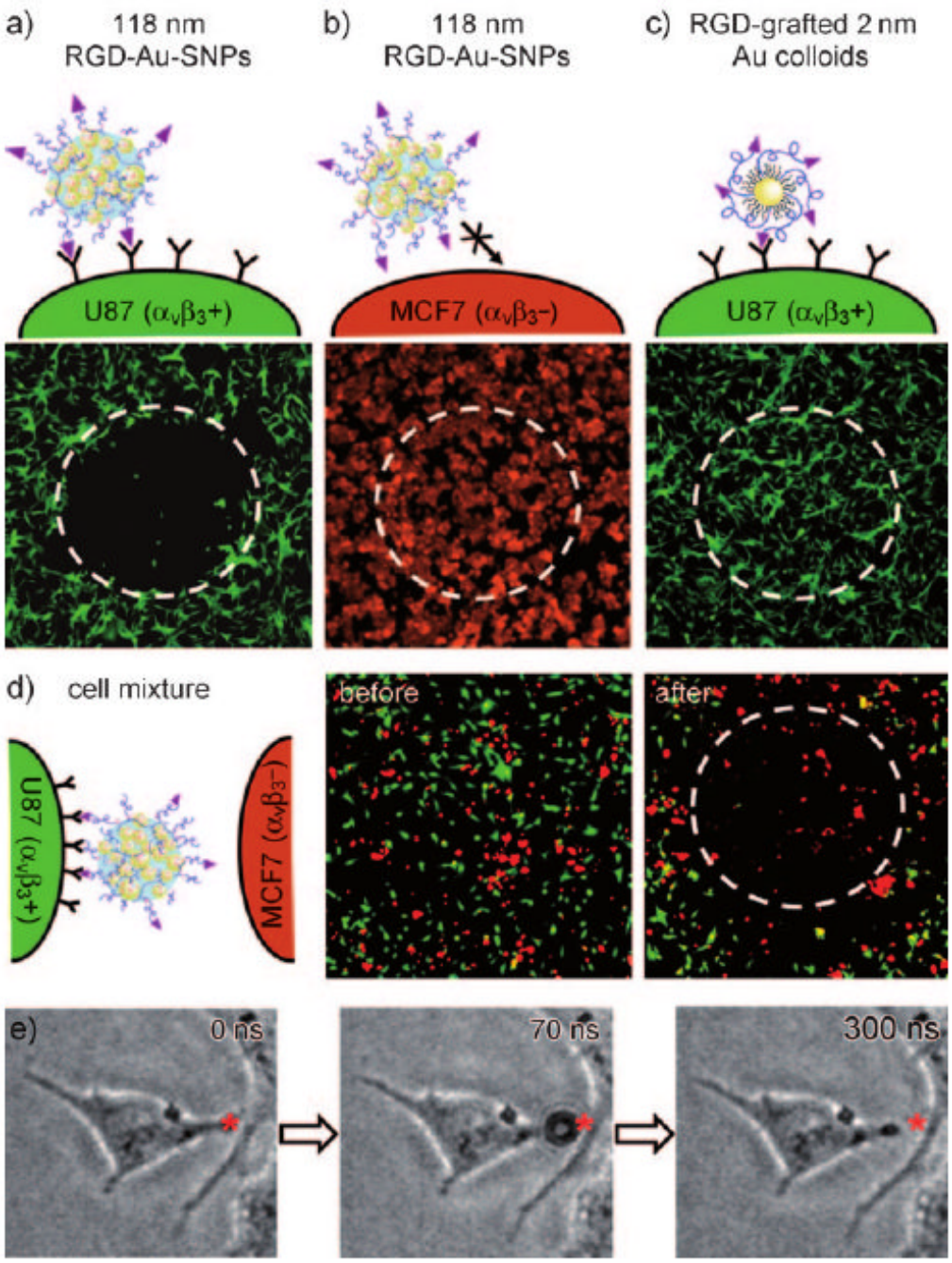

Figure 4.

a–c) Fluorescence micrographs of U87 cells ($\alpha_v\beta_3$ +, labeled green) treated with 118 nm RGD-Au-SNPs (a), MCF7 cells ($\alpha_v\beta_3$-, labeled red) treated with 118 nm RGD-Au-SNPs (b), and U87 cells treated with RGD-grafted 2 nm Au colloids (c) after irradiation with a pulsed laser (6 ns, 120 mJcm^{-2}). A mask was employed to confine the laser beam to a circular region with a diameter of 1 mm (as indicated by the white dashed circles). d) Fluorescence micrographs of a 1:1 mixture of U87 and MCF7 cells. After treatment with RGD-Au-SNPs and subsequent medium exchange, the cell mixture was irradiated with a pulsed laser. In the irradiated region after culture for 2 h, U87 cells (green) were depleted, whereas MCF7 cells (red) were left alive on the substrate. e) Time-resolved images of an $\alpha_v\beta_3$-positive U87 cell with a 118 nm RGD-

Au-SNP attached to it. Upon irradiation with the 6 ns pulsed laser (120 $mJcm^{-2}$), fast contraction of the cellular protrusion was observed as the result of the localized mechanical destruction caused by the formation of microbubbles.